p53 dynamically directs TFIID assembly on target gene promoters

Coleman, R. A.[1#], Qiao, Z.[1], Singh, S. K.[1], Peng, C. S.[1], Cianfrocco, M.[2], Zhang, Z.[3], Piasecka, A.[1], Aldeborgh, H.[1], Basishvili, G.[1], and Liu, W. L.[1]

[1]Gruss-Lipper Biophotonics Center, Department of Anatomy and Structural Biology, Albert Einstein College of Medicine, Bronx, NY 10461, USA.

[2]Department of Cellular and Molecular Medicine, University of California, San Diego, La Jolla, CA 92093, USA.

[3]Surrozen, 240 East Grand Avenue, 2nd Floor, South San Francisco, CA 94080, USA.

#To whom correspondence should be addressed. Department of Anatomy and Structural Biology, Albert Einstein College of Medicine, Bronx, NY 10461 Tel: 718-430-8623; Email: robert.coleman2@einstein.yu.edu

Abstract: 200 words, 1,195 characters
Introduction+Results+Discussion: 5,481 words, 30,987 characters
Figure Legends: 1029 words, 5,460 characters
Materials and Methods: 2,231 words, 11,857 characters

Running title: Binding dynamics of p53 and TFIID on DNA

Keywords: p53; TFIID; transcription; structure; single molecule microscopy

Abstract

The p53 tumor suppressor protein is a central regulator that turns on vast gene networks to maintain cellular integrity upon various stimuli. p53 activates transcription initiation in part by aiding recruitment of TFIID to the promoter. However, the precise means by which p53 dynamically interacts with TFIID to facilitate assembly on target gene promoters remains elusive. To address this key question, we have undertaken an integrated approach involving single molecule fluorescence microscopy, single particle cryo-electron microscopy, and biochemistry. Our real-time single molecule imaging demonstrates that TFIID alone binds poorly to native p53 target promoters. p53 unlocks TFIID's ability to bind DNA by increasing TFIID contacts with both the core promoter and a region surrounding p53's response element (RE). Analysis of single molecule dissociation kinetics reveals that TFIID interacts with promoters via transient and prolonged DNA binding modes that are each regulated by p53. Importantly, our structural work reveals that TFIID's conversion from a canonical form to a rearranged DNA-binding conformation is enhanced in the presence of DNA and p53. Notably, TFIID's interaction with DNA induces p53 to rapidly dissociate, effectively liberating the RE on the promoter. Collectively, these findings indicate that p53 dynamically escorts and loads the basal transcription machinery onto its target promoters.

Introduction

More than 50% of cancer patients harbor p53 mutations, highlighting the essential role of this protein in tumor suppression (1). To properly maintain genomic stability, p53 induces vast gene networks involved in diverse cellular pathways including cell cycle arrest, apoptosis and DNA repair (2). In response to various stress stimuli, p53 acts as a transcriptional activator that specifically binds consensus response elements (REs; two ten base-pair half sites, RRRCWWGYYY) within its target genes to directly stimulate gene expression (2). p53 utilizes its ability to non-specifically bind and slide along the DNA to expedite the search for target REs. (3). Upon recognition of its response genes, p53 facilitates transcription at least in part by targeting the TFIID-mediated transcription machinery to the promoter (4-7). TFIID is composed of TBP and 14 TBP-associated factors (TAFs). TFIID recognizes and binds multiple core promoter elements (e.g. the TATA box, Initiator, and downstream core promoter elements [DPE]) surrounding the transcription start site (TSS) (8). Once bound, TFIID serves as a central scaffold for six basal factors, including RNA Polymerase II, to form a pre-initiation complex (PIC) directing transcription initation. Importantly, without the assistance of activators such as p53, TFIID's core promoter recognition is weak and rate limiting for transcription initiation due to inefficient PIC assembly (9-16). As TFIID is responsible for transcription of at least ~90% of protein-coding genes (17), unraveling how p53 intervenes in this central step of the PIC assembly (i.e. TFIID's binding of promoter DNA) is essential for understanding mechanisms controlling gene-specific transcription initiation throughout the cell.

Previous biochemical studies of different activators (e.g. p53 and Zta) suggested a conserved albeit poorly characterized mechanism for facilitating transcription (10, 18, 19). It has been shown that p53 binds to its REs and enhances TFIID promoter recruitment via direct

90 contact with TBP and select TAFs (19, 20). However, p53 target genes have diverse spatial
91 arrangements of core promoter elements and p53 REs. Each target promoter also exhibits varied
92 affinities for p53 and TFIID (1). Therefore, it is unclear how distinct combinations of p53 REs
93 and core promoter elements affect the dynamics and the global architecture of TFIID assemblies
94 on target genes. Additional evidence has reported that p53 and other activators introduce
95 structural changes within TFIID when associated with TFIIA and DNA (10, 18, 19). This
96 activator-induced isomerization leads to enhanced TFIID binding to core promoter elements
97 downstream of the TSS (10, 18, 19). However, the structural mechanism of p53-mediated
98 isomerization of TFIID and its impact on PIC assembly is currently unknown.

99 Single molecule-based imaging has emerged as an advanced tool to discern complex
100 dynamic behavior of large multi-subunit protein assemblies involved in regulating gene
101 expression. A recent study utilizing real-time single molecule fluorescence microscopy provided
102 insight that TFIID's interaction with a synthetic core promoter DNA tightly correlates with
103 productive transcription (21). Another single molecule report uncovered TFIIB's dynamic
104 binding to TFIID at the promoter (22). Additional live cell studies also suggest that the PIC
105 composition is extraordinarily dynamic with the loading and promoter escape of RNA
106 Polymerase II occurring every ~ 4 to 9 seconds during bursts of transcription (23). How
107 activators such as p53 regulate TFIID's dynamic binding to native target DNA remains elusive.

108 Advanced single particle transmission electron microscopy (EM) has unraveled the three-
109 dimensional (3D) structures of TFIID and its co-complexes. Recent EM studies unmasked a
110 structural plasticity of TFIID, likely attributed to its promoter recognition activity (20, 24-27). In
111 particular, human TFIID features a "horseshoe" shape containing three major lobes (A, B & C)
112 and a well-defined central cavity (28, 29). Interestingly, we demonstrated that, in the absence of

113 DNA, three different activators, including p53, introduce a common set of local structural
114 changes in TFIID, such as movement of lobe A towards lobe B (20). Intriguingly, human TFIID
115 undergoes a significant structural rearrangement involving movement of Lobe A when bound to
116 a specific promoter DNA optimized for TFIID recognition (26, 27). It remains to be determined
117 if p53's facilitated movement of Lobe A results in a rearranged conformation of TFIID that
118 contributes to stable interaction between TFIID and DNA.

119 To uncover the mechanistic underpinnings of how p53 facilitates TFIID assembly on
120 promoter DNA, we exploited a combination of single molecule fluorescence microscopy,
121 biochemistry, and single particle cryo-EM analysis. These studies illuminate dynamic
122 interactions and static global molecular architectures of p53-induced TFIID assemblies on two
123 representative target genes (i.e. *hdm2* and *bax*). Our real-time single molecule studies show that
124 TFIID alone infrequently assembles onto these native p53 target promoters. TFIID/DNA binding
125 primarily occurs on the order of seconds. p53 facilitates TFIID's promoter recruitment by
126 enhancing multiple TFIID contacts throughout the core promoter and RE. Notably, p53 also
127 increases the percentage of TFIID molecules displaying long-lived DNA binding. Consistent
128 with our single molecule studies, EM structural analysis reveals that conversion of canonical
129 TFIID to a rearranged DNA binding conformation is enhanced in the presence of p53 and DNA.
130 TFIID/DNA binding induces p53 dissociation, effectively "liberating" the RE to allow p53-
131 mediated recruitment of additional factors involved in PIC formation. Therefore, proper response
132 to divergent stress signals involves conserved structural mechanisms relating to p53's ability to
133 dynamically stimulate TFIID's interaction with various target promoters.
134

134 **Results**

135 ***TFIID association with native target genes in the presence of p53***

136 We sought to further understand the molecular mechanism pertaining to activator-
137 mediated enhancement of TFIID's ability to bind DNA. Thus, dynamic interactions between
138 p53, TFIID and promoter DNA were characterized via a single molecule co-localization assay
139 using Total Internal Reflection Fluorescence Microscopy (TIRF) (Figure 1A)(21, 22). Over the
140 first 15' of binding, Quantum dot-labeled TFIID (QD-TFIID) associated with only 1.5% of the
141 Cy3/Cy5-labeled native wild-type *hdm2* promoter DNA in the absence of p53 (Figure 1B and
142 Supplemental Figure S1, left panel), revealing a low intrinsic affinity of TFIID for DNA.
143 Increasing the time between addition of TFIID to the DNA and the imaging of binding did not
144 improve co-localization efficiencies, suggesting that reactions are at equilibrium (data not
145 shown). This finding indicates that, at low concentrations (~1nM), TFIID inefficiently
146 recognizes DNA. On the other hand, increased binding of TFIID to DNA was observed in our
147 bulk biochemical assembly assays when much higher concentrations (100-600nM) were used as
148 in Supplemental Figure S6B.

149 Upon addition of p53, a clear enhancement of TFIID's association with the *bax* or *hdm2*
150 promoter DNA was observed (Figure 1B). This result is consistent with a general increase of
151 DNA retained by TFIID in the presence of p53 in our bulk biochemical assays (Supplemental
152 Figure S6B). A control experiment detected no p53-mediated co-localization of DNA with the
153 Quantum dot-labeled TAF1 antibody (0.2 ± 0.07% co-localization) in the absence of TFIID (data
154 not shown). Therefore p53's significant enhancement TFIID/DNA association is likely due to the
155 direct interaction between p53 and TFIID.

156 To directly address the role of the p53 RE and core promoter elements in p53-mediated
157 TFIID/DNA binding, three mutant *hdm2* DNA templates were analyzed with the same real-time
158 co-localization assay (Figure 1B). The first mutant *hdm2* DNA template (i.e. Mu RE) harbors
159 mutations in the response elements known to impair p53's sequence-specific interactions (30). A
160 mild but significant decrease of TFIID's association with DNA was observed on the mutant p53
161 RE template (Figure 1B). This result suggests that enhancement of TFIID/DNA binding can
162 occur via a mechanism that is independent of p53/RE contacts.

163 To assess the impact of the core promoter in p53-mediated TFIID/DNA binding,
164 mutations (i.e. Mutant Core) known to weaken TFIID binding and inhibit transcription (22, 31)
165 were exploited. Upon addition of p53, TFIID's association with the mutant core template was
166 further reduced compared to the wild-type promoter (Figure 1B). As expected, when both the
167 p53 RE and core promoter elements were altered (i.e. Mu RE/Co), TFIID/DNA co-localization
168 was further decreased (Figure 1B). These results indicate that the p53 RE and core promoter
169 elements were both required for optimial association of TFIID with p53 target gene promoters.

170 ***p53 regulates TFIID/DNA contacts within the core promoter and p53 response elements***

171 As an alternative approach to study p53-mediated TFIID/DNA binding, we developed an
172 in vitro formaldehyde-crosslinking/exonuclease mapping assay (xlink-Exo). Our strategy was
173 adapted from a well-established strategy (ChIP-exo) to map out protein/DNA contacts of
174 transcription factors in vivo at near base-pair resolution (32). Based on this analysis, TFIID
175 makes extensive contacts with well-characterized core promoter elements (i.e. TATA, InR, MTE
176 and DPE) on the wild-type *hdm2* DNA (Figure 1C, top panels). Addition of p53 led to elevated
177 crosslinking of TFIID to the wild-type core promoter with select elements showing much larger
178 changes (i.e. TATA, InR) than others (i.e. MTE/DPE) (top panels). Consistent with our single

179 molecule data, p53 increases the specific binding of TFIID to the core promoter. Importantly,
180 there was a clear reduction in p53's ability to enhance contacts within mutated core promoter
181 elements (Figure 1C, bottom panels and Supplemental Figure S2A). This finding is consistent
182 with our single molecule assay showing reduced TFIID/DNA co-localization on the mutant core
183 promoter (Figure 1B). Interestingly, p53 slightly increases TFIID's contacts within the -4 and
184 +11 regions on these mutant core promoters (Figure 1C, bottom panel and Supplementary Figure
185 S2A). Thus our mutantions don't completely eliminate TFIID/core promoter contacts and may
186 explain why a small percentage of TFIID is still bound to the mutant promoters in our single
187 molecule assays (Figure 1B).

188 In addition to these well-established contacts, our xlink-Exo assays also mapped
189 TFIID/DNA interactions far upstream of TATA (-55 to -137) and downstream of the DPE (~
190 +37 to +68) (Figure 1C, top panel). This result is consistent with previous DNAse I footprinting
191 studies reporting TFIID/DNA interactions upstream of TATA (-40 to -140) and downstream of
192 the DPE (+32 to +68) at similar positions on different promoters (26, 33, 34). Many of these
193 upstream and downstream TFIID contacts were enhanced when p53 was co-present on the wild-
194 type *hdm2* promoter (Figure 1C). Moreover, some of TFIID's upstream contacts (i.e. -55 to -88)
195 reside within the p53 RE on the wild-type promoter even in the absence of p53 (Figure 1C, top
196 panels). Mutations of the p53 RE led to a loss of TFIID's contacts at -61 and -88, suggesting that
197 TFIID recognizes specific sequences within the p53 RE (Figure 1C, bottom panels and
198 Supplemental Figure S2B). Furthermore, a number of upstream TFIID contacts (-61, -79, and -
199 88/-90) were also abrogated on the mutant core promoter (Supplementary Figure S2). This
200 suggests that these novel upstream DNA contacts arise from TFIID's interaction with the TATA,

201 InR and DPE sequences. Therefore, TFIID may utilize additional uncharacterized elements to
202 recognize promoters.

203 ***p53 modulates the prolonged association of TFIID with DNA***

204 In addition to p53's ability to stimulate TFIID/DNA association, we sought to test if p53
205 could also stabilize TFIID's binding to DNA. Therefore, the amount of time that QD-TFIID
206 remains bound to a single promoter DNA before dissociating (i.e. residence time) with and
207 without p53 was examined (Figure 2A). In the absence of p53, two populations of DNA-bound
208 TFIID complexes displaying distinct residence times were detected on the wild-type *hdm2*
209 template (Figure 2B). The majority (78%) of TFIID/DNA binding events were short-lived
210 (average residence time of 6.6 ± 0.4 seconds) in the absence of p53 (Figure 2B, left panel).
211 Notably, p53 significantly increases the percentage of long-lived TFIID/DNA bound complexes
212 from 22% to 64% (Figure 2B, left versus right panel). Furthermore, p53 prolongs the residence
213 time of both the short and long-lived TFIID/DNA binding events (Figure 2C). TFIID also
214 displayed a similar stability profile on the *bax* promoter in the presence of p53 (Supplemental
215 Figure S3). These results suggest that TFIID interacts with DNA via two intrinsic binding modes
216 that can be modulated by p53.

217 We next defined how the RE and core promoter elements might regulate the relative
218 proportion of these two TFIID/DNA binding populations in the presence of p53. Disruption of
219 the p53 binding site on the *hdm2* promoter (Mu RE) had little effect on the distribution between
220 these two populations (Figure 2D). This indicates that a p53-mediated increase in the percentage
221 of TFIID molecules displaying long-lived DNA binding does not solely require contacts with the
222 RE. In contrast, mutation of the core promoter region (Mu Core) reduced the percentage of
223 TFIID molecules in the long-lived DNA binding population (Figure 2D). Alteration of the p53

224 binding site and the core promoter elements (Mu RE/Co) further lowered the percentage of the
225 TFIID's long-lived DNA binding population (Figure 2D). These data suggest that the TFIID's
226 long-lived DNA binding mode was related primarily to recognition of the core promoter with
227 p53/RE interactions providing additional stability post-recruitment to the DNA.

228 Our results also reveal that p53 RE and core promoter mutations also impacted TFIID's
229 residence time on DNA. Mutation of the p53 RE (Mu RE) predominantly decreased the
230 residence time of TFIID's long-lived DNA binding without significantly affecting the short-lived
231 events (Supplementary Figure S4B). Therefore, interactions between p53 and its RE are required
232 for maximal stability of TFIID/DNA contacts on native target promoters. On the mutant core
233 promoter (Mu Core) residence times for both the long- and short-lived TFIID/DNA binding
234 events were also significantly reduced (Supplementary Figure S4). Thus, both DNA binding
235 modes were related to core promoter recognition. Mutation of both the p53 RE and core
236 promoter were changed (Mu RE/Co) had little effect of TFIID's residence time on DNA
237 (Supplementary Figure S4B). These results suggest that mutation of both the RE and core
238 promoter elements primarily effects TFIID's distribution between short and long-lived DNA
239 binding modes (Figure 2D). Together with the single molecule data, our xlink-Exo studies
240 suggest that TFIID's remaining minimal contacts on our mutant promoter are sufficient to anchor
241 short-lived TFIID binding to DNA.

242 ***p53/target promoter interactions in the presence of TFIID***

243 Our previous report documented that a TFIID variant could cooperatively increase the
244 binding of the activator c-Jun to its binding site on promoter DNA (24). To quantitatively assess
245 if this was the case for p53, the dissociation dynamics of fluorescently labeled-p53/DNA
246 interactions with or without TFIID were examined (Figure 3). In the absence of TFIID, p53

247 primarily displayed two populations of distinct binding events on the wild-type *hdm2* template
248 (i.e. long-lived [avg = 33.1 ± 3.9”] and short-lived [avg = 7.4 ± 0.7”], Figure 3A, left panel).
249 Since earlier reports showed that p53 can bind DNA non-specifically (35, 36), we hypothesized
250 that these short-lived p53/DNA binding events were non-specific interactions. To test our
251 hypothesis, the same experiments were performed using the mutant p53 RE template (right
252 panel). Indeed, disruption of p53’s sequence-specific binding sties on DNA led to a single short-
253 lived population (avg = 6.8 ± 0.7”). Based upon this result, the long-lived p53/DNA binding
254 events most likely represent sequence-specific interactions (left panel), whereas the short-lived
255 p53/DNA binding events are non-specific in nature. Alternatively, these short-lived events could
256 represent interactions with an unknown lower affinity p53 binding site in the promoter or binding
257 of dimeric p53 to concensus half-sites within the mutant RE. It is of note that photobleaching of
258 the fluorescently labeled p53 did not affect our results, since similar residence times were
259 observed with multiple dyes of differing photostability (data not shown). In addition, a previous
260 study detected similar short residence times of ~10-12” for p53 bound to a consensus site (37).
261 Collectively, these findings indicate that p53 dynamically interacts with DNA via both specific
262 and non-specific interactions.

263 Importantly, addition of TFIID resulted in a single population of p53 bound to wild-type
264 DNA with an “intermediate-lived” residence time distinct from the two populations observed
265 with p53 alone (Figure 3B). Furthermore, we noticed that fitting of the data showed slight
266 deviations from an exponential decay model. A previous study indicated that the existence of
267 complex multi-step dissociation events could be discerned using a gamma distribution model to
268 fit single molecule data (38). Indeed, we found that a gamma distribution model better represents
269 the data (Figure 3B, right panel). This analysis shows that in the presence of TFIID, p53

270 dissociates from the DNA in ~2 steps. Each step contains roughly equivalent residence times of
271 8.2 seconds per step (average total time = 14.8 ± 1.5”). Moreover, single step dissociation
272 kinetics was observed for p53 alone based upon gamma distribution fitting (data not shown).
273 Therefore, TFIID alters both the rate and number of kinetic steps involved in p53’s dissociation
274 from promoter DNA.

275 Mutation of the p53 RE further reduces p53’s residence time on DNA in the presence of
276 TFIID (Supplemental Figure S5A, left panel versus Figure 3B, right panel). Disruption of
277 TFIID’s interaction with the TATA, InR and DPE elements on the mutant p53 RE/Co DNA
278 template does not lead to a further decrease in p53’s residence time (Supplemental Figure S5A
279 versus S5B). Fitting of the dissociation data on the mutant templates to a gamma distribution
280 yielded poor fits, suggesting single step dissociation kinetics for p53 on these mutant promoters
281 (Supplemental Figures S5A and S5B, right panels).

282 Overall, these data suggest that TFIID binding to DNA can influence p53’s stability at
283 the RE. TFIID’s interaction with p53 likley promotes the dissociation of p53 bound to specific
284 sequences in the promoter (Figure 3C, left panel). Importantly, the average time of p53 bound to
285 the wild-type *hdm2* template (~15”) is significantly shorter than TFIID’s long-lived DNA
286 binding time (~100”) (Figure 3C, right panel). These dynamic studies strongly suggest that p53
287 transiently escorts TFIID to the promoter DNA. Importantly, p53 is not required to remain bound
288 for TFIID’s maximum stability on promoter DNA.

289 ***The conformational status of TFIID when co-present with p53 and promoter DNA***

290 A recent cryo-EM study discovered that human TFIID switches from a canonical to a
291 rearranged conformation upon binding to the Super Core Promoter (SCP), a DNA fragment
292 optimized for interaction with TFIID (26, 31). Thus far our single molecule data indicates that

293 p53 stimulates binding of TFIID to DNA. Therefore, we hypothesized that TFIID could form a
294 rearranged DNA binding conformation with p53 and promoter DNA. Therefore, we set out to
295 determine TFIID's global structural architecture when p53 and target promoter DNA were
296 present. As the first step, unbiased reference-free 2D classification experiments were performed
297 to examine conformational states of TFIID in the presence of p53 or p53/*bax* DNA (Figure 4A).
298 The movement of Lobe A from Lobe C to Lobe B is the hallmark of the rearranged DNA
299 binding conformation of TFIID (26). Therefore, three conformational states of TFIID
300 represented by corresponding views of 2D class averages were defined based upon the position
301 of Lobe A relative to Lobes C and B (top panels, i.e. canonical, transition, and rearranged state).
302 We found that addition of p53 led to an elevated percentage of particles within the corresponding
303 view displaying the rearranged TFIID form compared to TFIID alone (Figure 4A, bottom panel).
304 This finding implies that the formation of TFIID's rearranged state is affected by p53. This result
305 is consistent with conformational changes observed in our previous negative stained structure of
306 a TFIID/p53 co-complex (20). Furthermore, the 2D classification analysis showed that the
307 populations of both the transition and rearranged forms increased when p53 and DNA was added
308 (bottom panel). Therefore, these findings suggest that TFIID's conformational switches can be
309 regulated via target gene promoters and/or its interaction with p53.

310 A previous biochemical study reported that p53 stimulated the assembly of TFIIA and
311 TFIID on a synthetic promoter DNA (19). Interestingly, unlike p53, TFIIA alone promotes the
312 canonical form of TFIID (26). Thus, to assess the structural framework of TFIID in the presence
313 of p53 and TFIIA, two TFIID/p53/TFIIA assemblies on the native *hdm2* and *bax* promoter
314 fragments (488 bp and 500 bp) were obtained (Supplemental Figure S6). To visualize both
315 conformations and the DNA, cryo-EM data of these assemblies were obtained for reference-free

316 2D classification analysis. Some class averages showing the presence of promoter DNA
317 spanning the central cavity of TFIID were observed (Figure 4B). Moreover, both assemblies
318 displayed a similar rearranged TFIID architecture, despite the different organization of their
319 promoters. Each template harbors non-consensus core promoter elements with different spatial
320 arrangements between TATA and the Initiator (Figure 1B, top panel) (8, 39, 40). Combined with
321 our 2D classification analysis (Figure 4A), these structural studies indicate that TFIID binds
322 DNA in a common rearranged conformation in the presence of p53 and TFIIA.

323 Next, to identify the relative DNA orientation and any distinct structural features, we
324 compared the class averages of our two assemblies with the previous structural analysis of
325 TFIID/TFIIA/SCP DNA containing a mapped DNA orientation (26). Our co-complexes
326 displayed clear views of TFIID stably bound to the *bax* DNA downstream of the TSS (Figure
327 4C, top two rows). In contrast, upstream promoter DNA was weakly visible in our averages
328 (middle panel). These results suggest that the p53 RE upstream of the TATA box element is
329 flexible within the co-complex. To define promoter DNA upstream of TATA, focused
330 classification on a class average displaying flexible upstream DNA (middle panel) was
331 performed as previously described (26). This analysis revealed a clear density for the upstream
332 promoter DNA (highlighted by yellow arrow, bottom panel). Given the strong density for
333 downstream DNA within the assembly, these results imply that TFIID serves as a strong anchor
334 for downstream promoter DNA during PIC assembly.

335 The 2D class averages of TFIID/DNA/p53/TFIIA assemblies exhibit a similar topology
336 to the averages from TFIID/TFIIA bound to the SCP DNA (refer to Figure 3 in (26)) raising two
337 major points. First, TFIID adapts a common DNA binding conformation to bind various p53
338 target gene promoters. Second, structural rearrangements within TFIID related to DNA binding

339 may cause p53 to dissociate, as supported by our single molecule dynamics results (Figure 3). To
340 test these hypotheses, single particle 3D reconstruction was conducted to determine the 3D
341 structure of the TFIID/TFIIA/p53/*bax* DNA co-complex (Supplemental Figure S7A). The overall
342 structural architecture of our co-complex is comparable to the 3D structure of TFIID/TFIIA/SCP
343 DNA. Our 3D reconstruction was also verified by analyzing its 3D projections with their
344 matching reference-free 2D averages (Supplemental Figure S7B). The same observation was also
345 obtained with the 3D structure of the TFIID/TFIIA/p53/*hdm2* promoter DNA (Supplemental
346 Figure S8). These results suggest that TFIID utilizes one common rearranged form to bind
347 various promoters.

348 Our 3D reconstruction did not reveal any prominent extra densities that would most
349 likely represent the p53 protein. This indeed suggests that p53 dissociates from the
350 TFIID/TFIIA/*bax* DNA co-complex. Alternatively, p53 could have a transient interaction with
351 the assembly, which led to the EM density being averaged out during analysis. Since we
352 previously determined the 3D structure of the p53 bound TFIID co-complex without DNA (20),
353 we attempted to capture the p53-bound state of TFIID in the cryo-EM dataset of our
354 TFIID/TFIIA/p53/*bax* DNA assembly. Thus, 3D reconstructions were performed using the
355 structure of p53/TFIID as an initial reference volume. A poor resolution 3D reconstruction of
356 p53/TFIID was obtained, indicating a small subset of the single cryo-EM particles (Supplemental
357 Figure S9). This observation suggests that the majority of TFIID complexes have switched to
358 the p53-free, DNA-bound state when p53 and DNA were co-present. Collectively, these
359 structural studies support the observations from our single molecule analyses, illustrating that
360 p53 dissociates from TFIID and DNA when recruited to target promoters. Our work also implies
361 that when p53 stimulates TFIID binding to DNA, a common rearranged DNA binding scaffold is

362 formed on various target genes.

363

363 **Discussion**

364 ***TFIID infrequently interacts with native p53 target genes in the absence of additional factors***

365 Our single molecule assays reveal that TFIID poorly associates with native p53 target
366 promoters in the absence of p53 (Figure 1B). TFIID's inefficient DNA binding activity may be
367 one way to prevent spurious basal expression of these stress response genes. TFIID/promoter
368 interactions are likely repressed in part due to the TAF1 N-terminal domain (TAND) which
369 occupies TBP's concave DNA binding surface (41-44). This TAF1/TBP interaction is also
370 thought to control the TFIID's global conformation to regulate promoter interactions. TFIID's
371 canonical conformation is non-permissive to DNA binding (26, 27) (Figure 5 top panel, left
372 side). Researchers postulate that the TAF1 TAND acts to tether TBP to TFIID's lobe C in the
373 canonical form (27). Large-scale structural rearrangement of TFIID dramtically shifts TBP's
374 positon within TFIID to allow simultaneous contact of TBP with the upstream TATA and TAF1
375 with downstream core promoter elements (Figure 5 top panel, right side). Thus TAF1/TBP
376 interactions repress the large-scale structural rearrangement within TFIID required for TBP to
377 bind the TATA element in a core promoter.

378 TFIID's infrequent association with p53 target gene promoters occurs via distinct short
379 and long-lived DNA binding modes (Figures 2B, 2C and Supplementary Figure S4B). The
380 majority (78%) of these TFIID/DNA binding events last just a few seconds (~7") (Figures 1B,
381 2B and 2D). This short-lived DNA binding population may represent a transient non-productive
382 TFIID encounter complex in the canonical form where TAF1 prevents stable TBP/TATA
383 interactions (Figure 5). In such a scenario, TAF contacts with the initiator and DPE may be
384 sufficient to temporarily anchor TFIID to DNA. Due to this transient dynamic interaction

385 behavior, we were likely unable to obtain the 3D structure of those short-lived DNA-bound
386 TFIID complexes via cryo-EM.

387 ***DNA binding and structural features of TFIID are regulated by p53***

388 A number of factors, including activators (i.e. c-Jun and VP16) and TFIIA, can stimulate
389 TFIID/promoter binding by de-repressing the TAF1-mediated inhibition of TBP (19, 45-48).
390 TFIIA has also been found to aid conversion of canonical TFIID to the rearranged DNA binding
391 form likely via disruption of TBP/TAF1 TAND interactions (26, 27). It was previously unclear if
392 activators could also promote structural rearrangement of TFIID to stimulate promoter
393 association. Our past work has shown that p53 binds stably to TFIID and targets TAF1 in the
394 absence of DNA (20). We also found that p53's interaction with TFIID also results in movement
395 of Lobe A towards Lobe B in a manner analogous to a structurally rearranged DNA binding form
396 of TFIID (20). Therefore we postulated that DNA binding may be increased in this structurally
397 rearranged pre-assembled p53/TFIID complex. Indeed our single molecule data along with
398 previous bulk biochemical experiments indicate that p53 can dramatically stimulate the binding
399 of TFIID to DNA (Figure 1B and (19)). We also find that conversion of canonical TFIID to the
400 structurally rearranged form is enhanced in the presence of p53 and DNA (Figure 4A). Thus we
401 speculate that p53, whose acidic activation domain is highly homologous to VP16 (49), may
402 potentially disrupt TAF1/TBP interactions to aid in TFIID structural rearrangement and DNA
403 binding (Figure 5, bottom panel).

404 ***p53 promotes isomerization of TFIID to stimulate long-lived binding to DNA***

405 Cryo-EM of a TFIID/TFIIA/DNA complex has revealed a number of TBP/TAF contacts
406 with core promoter elements spanning from ~ -33 to +32bp surrounding the transcription start
407 site (27). Many of these contacts, especially TBP/TATA, are only possible due to TFIID's

408 structural rearrangement or isomerization upon DNA binding. Therefore we anticipate that the
409 p53-mediated binding of TFIID to DNA is also likely a multi-step isomerization process
410 involving contacts with multiple core promoter elements (Figure 5, bottom panel). Indeed our x-
411 link Exo analysis revealed numerous TFIID crosslinks throughout the promoter that are
412 enhanced by p53 (Figure 1C). Many of these TFIID/*hdm2* DNA contacts were strictly conserved
413 in the TFIID/TFIIA/super core promoter DNA cryo-EM structure (27). Consistently, the
414 architectures of TFIID bound to the *hdm2* and supercore promoters are equivalent (Supplemental
415 Figures S7 and S8). This suggests that TFIID in the presence of p53 can specifically bind our
416 native *hdm2* promoter to adopt a common DNA binding conformation.

417 In the presence of p53, TFIID associates with DNA robustly. Analysis of single molecule
418 dissociation kinetics also revealed two TFIID/core promoter DNA binding modes with
419 interactions predominantly being long-lived (~100") (Figures 2B and 2D). Therefore, p53 shifts
420 the TFIID population from short to long-lived DNA binding, likely acting to facilitate TFIID's
421 known isomerization on promoters (Figure 5, bottom panel). This isomerization step may
422 possibly permit stable interaction of TFIID with the upstream DNA, TATA box and downstream
423 DNA resulting in long-lived DNA binding (Figure 5, bottom panel). We speculate that the p53-
424 mediated long-lived DNA-bound TFIID complex is structurally related to the stable
425 TFIID/TFIIA/promoter DNA complex depicted in our cryo-EM studies. In support of this model,
426 previous biochemical assays have shown that activators induce conformational changes within
427 TFIID that enhance multiple contacts with promoter sequences downstream of the TSS (10).

428 Mutation of the p53 RE only affected the residence time of TFIID's long-lived DNA
429 binding population (Supplementary Figure S3). Importantly, the percentage of long-lived DNA
430 binding events was essentially unchanged on the mutant RE template (Figure 2D). This suggests

431 that isomerization of TFIID does not depend on p53 contacts with the RE. Given that distinct
432 TFIID contacts surrounding the p53 RE were identified via our xlink-Exo assays (Figure 1C), we
433 speculate that this upstream DNA is involved in both binding p53 and stabilizing interaction of
434 an isomerized form of TFIID with the promoter. These upstream contacts may be possibly
435 mediated by the TAF4 subunit of TFIID, which was previously shown to bind ~70 bp of DNA
436 with a weak sequence preference (50).

437 ***TFIID isomerization upon DNA binding liberates p53 from the RE***

438 Our single molecule data indicate that TFIID reduces p53's residence time on DNA
439 (Figures 3A and 3B). This result is consistent with previous DNAse I footprinting studies
440 showing decreased binding of p53 to REs in the presence of TFIID (19). More importantly,
441 p53's residence time on DNA is 6.7 fold shorter (~15") than TFIID's (~100") (Figure 3C, right
442 panel). Therefore p53 disengages the promoter before TFIID during long-lived DNA binding
443 events. In our EM structures, we are also unable to detect density associated with p53 in the
444 rearranged DNA bound TFIID further confirming our single molecule findings (Supplemental
445 Figures S7, S8 and S9). Previous structural analysis shows that p53 bridges lobes A and C of
446 TFIID in the absence of DNA (20). Thus, we speculate lobe A's movement away from lobe C
447 upon DNA binding disrupts p53/TFIID contacts inducing p53's dissociation from the assembly
448 (Figure 5, bottom panel).

449 While p53 dissociates from the TFIID/DNA scaffold, it is highly likely that p53 will
450 rapidly re-associate with the complex, particularly at the high concentrations (600nM) used in
451 Supplementary Figure S6. We suspect that p53's rapid removal could consequently lead to a
452 faster "repurposing" of the RE for additional rounds of p53-mediated recruitment of other basal
453 transcription factors such as TFIIB (51, 52), RNA Pol II (53), and TFIIH (49, 54, 55). In this

454 scenario, stable prolonged binding of p53 to a TFIID/DNA complex would negatively regulate
455 PIC formation, because p53 would occupy the RE and inhibit subsequent recruitment of a
456 p53/basal factor co-complex.

457 ***TFIID/promoter binding dynamics in relation to transcriptional burst kinetics***

458 Once p53 loads TFIID onto our native p53 target gene promoters, TFIID remains bound
459 for only approximately 100 seconds likely due to interactions with suboptimal or non-consensus
460 core promoter elements (Figure 2). Notably, our residence times for TFIID at the promoter were
461 measured in the absence of additional PIC components. Most likely, additional factors such as
462 TFIIA, TFIIF, and RNA Polymerase II will alter the stability of TFIID and p53 as the PIC forms
463 on promoter DNA. However, recent in vivo work suggests that transcription complex formation
464 is highly dynamic. Consistent with our data, yeast TBP occupies the HSC82 heat shock promoter
465 for 60 seconds in vivo (56). In human tissue culture cells, RNA Polymerase II loads onto
466 promoters every ~4 to 9 seconds to form convoys on an active gene (23). These bursts of RNA
467 Polymerase II convoys last for approximately 100 seconds before the promoter becomes inactive
468 again (23). Therefore it is tempting to speculate that the long-lived TFIID residency (~100
469 seconds) on our native target promoters could be related to RNA Polymerase II convoy
470 formation (~100 seconds) and transcriptional bursting. TFIID's dynamic binding to promoters
471 could be a mechanism to allow rapid shut down of stress response gene expression after re-
472 establishment of cellular homeostasis.

473 TFIID can also direct infrequent loading of RNA Polymerase II convoys on mutant
474 TATA containing promoters leading to bursts of transcription (23). Interestingly, the duration of
475 RNA Polymerase II convoys on the mutant TATA promoter is only slightly less than that on a
476 wild-type TATA template (~60-80 seconds) (23). Our study also revealed infrequent p53

477 mediated binding of TFIID on our mutant core promoter DNA lasting for a significantly long
478 time (~64 seconds) (Figure 2D and Supplementary Figure S3). Therefore we suspect that TFIID
479 stably loaded onto our mutant core DNA is fully competent to direct low levels of infrequent
480 transcription. Overall, our studies indicate that p53, and potentially activators in general, serve as
481 escorts to dynamically recruit and load the basal transcription machinery onto DNA via complex
482 interactions between the RE, the core promoter and bound basal factors (i.e. TFIID). Our work
483 also reveals how p53 stimulates TFIID binding to different promoters that comprise variable
484 arrangements of p53 binding sites and core promoter elements. More importantly, our combined
485 functional and structural studies are crucial for understanding how eukaryotic transcription
486 complexes dynamically assemble on different protein-coding gene promoters.
487
488
489

489 **Materials and Methods**
490
491 **Reagents and protein purification**
492
493 Experimental details, including reagents, protein purification of the p53/TFIID/TFIIA/DNA
494 co-complexes and fluorescent-labeled proteins/DNA used in this study along with our custom-
495 built TIRF microscope setup, are described in the Supplemental Materials.

496 **In vitro immuno-assembly assay**

497 HeLa cells (32 liters) were grown in suspension culture with 1X DMEM plus 5% newborn calf
498 serum for each assay. Nuclear extract was prepared and fractionated with phosphocellulose P11
499 (P-Cell) resins exactly as previously described (20). P-Cell column fractions eluting at 1M
500 KCl/HEMG buffer (pH 7.9, [20 mM Hepes, 0.2 mM EDTA, 2 mM $MgCl_2$, 10% Glycerol, 1 mM
501 DTT and 0.5 mM PMSF]) were pooled, dialyzed to 0.3 M KCl/HEMG buffer, added with final
502 concentration of 0.1% NP40, and then immunoprecipitated overnight at 4°C with an anti-TAF4
503 mAb covalently conjugated to Protein G Sepharose beads (GE Healthcare Life Sciences). TAF4-
504 immunoprecipitates were extensively washed with 0.65 M KCl/HEMG buffer, 0.3 M
505 KCl/HEMG buffer and 0.1M KCl/HEMG buffer (containing 0.05% NP40 buffer and 10 μM
506 Leupeptin) and split into four assembly reactions as indicated in Figure 1. Three reactions of
507 TFIID-bound resins were incubated with 6-fold molar excess of promoter DNA. Next, two
508 TFIID/DNA reactions were further added with 10-fold molar excess of p53 alone and/or TFIIA.
509 Four total reactions were incubated at 4°C for 2 hours prior to elution of the co-complex from the
510 TAF4 mAb affinity resin. TFIID/factor/DNA-bound resins were washed 5 times with 0.1 M
511 KCl/HEMG buffer (containing 0.1% NP40 and 10 μM Leupeptin) followed by elution with a
512 peptide (1 mg/ml) in 0.1 M KCl/HEMG buffer (plus 0.1% NP40 and 10 μM Leupeptin)
513 recognized by the TAF4 mAb. Eluates were analyzed with 4-12% SDS-PAGE (NuPage gel
514 system, Thermo Fisher) and visualized by silver staining analysis.
515

516 **Xlink-Exo assay**

517 Exonuclease assays were carried out in 10µl reactions containing a modified 50 mM KCl/HEMG
518 buffer (pH 7.9, [12.5 mM Hepes, 0.05 mM EDTA, 6.25 mM $MgCl_2$, 5% glycerol] plus 1% DTT,
519 0.05 M PMSF, and 0.01% NP-40), IRdye800 (IDT) antisense strand labeled *hdm2* promoter
520 DNA (9nM) , p53 (90nM, monomer), and TFIID (4nM). After incubation at room temperature
521 for 20', reactions were crosslinked with formaldehyde (1% final) for 5' and stopped by addition
522 of Tris-HCl (100mM final, pH 8.0). Next, each reaction was mixed with Exonuclease III (50
523 Units, NEB diluted in a buffer containing $MgCl_2$ [16.25 mM final]), and incubated at 37°C for 1
524 hour. Proteinase K (10µg) was then added into each reaction and incubated at 70°C for 3 hours.
525 Reactions were mixed in formamide loading dye, heated at 95°C and resolved on a 8%
526 Polyacrylamide-TBE gel containing 7M urea. A series of known 5' truncated IRdye800 (IDT)
527 antisense strand labeled wild-type *hdm2* DNA fragments were generated and used as molecular
528 standards to determine the size of Exonuclease digested bands seen on our mapping gels.

529

530 **TIRF Single Molecule Imaging**

531 Passivated glass coverslips (see Supplemental materials) were assembled into a multichannel
532 flow cell using double sided tape (3M). Flow cells were mounted on the microscope and
533 streptavidin was added to the flow cell to coat surfaces. Each flow cell holds ~50 ul of sample.
534 Reference beads that serve as fiducial marks were immobilized on the bottom surface of the flow
535 cell. Biotinylated Cy3/Cy5 promoter DNA in 1X PBS was then loaded into the flow cell and
536 bound over time specifically to the streptavidin that was non-covalently attached through biotin
537 linkages on the top and bottom surfaces. Promoter DNA templates were briefly imaged at 3HZ to
538 determine surface attached DNA densities that were sufficient for localization of single DNA
539 molecules. Unbound biotinylated Cy3/Cy5 promoter DNA was washed away. Promoter DNA

540 templates were then imaged at 3HZ. The surface attached Cy3/Cy5 promoter DNA was then
541 photobleached. Reactivation of the Cy3/Cy5-labeled promoter DNA was not evident over the
542 timescale of our experiments (typically 15-20 minutes). Qdot 565-labeled TFIID (1 nM) in the
543 absence and presence of unlabeled p53 (8 nM, monomer) was then added to the flow cell in a
544 modified 50 mM KCl/HEMG buffer (pH 7.9, [12.5 mM Hepes, 0.05 mM EDTA, 6.25 mM
545 $MgCl_2$, 5% glycerol] plus 1% DTT, 0.05 M PMSF, and 0.01% NP-40) and immediately imaged
546 at 3Hz at 23°C. An oxygen scavenging system consisting of 0.4% b-D-Glucose, 1 mg/ml glucose
547 oxidase (Sigma), and 0.4 mg/ml catalase (Sigma) was used for imaging. For experiments to
548 measure p53's interaction with promoter DNA, AlexaFluor 555, Cy3- or Cy5-labeled p53 (8nM,
549 monomer) in the absence or presence of unlabeled TFIID (1 nM) was added to the flow cell
550 containing surfaced attached mapped promoter DNA and immediately imaged at 3Hz.
551 AlexaFluor 555, Cy3- and Cy5-labeled p53 had equivalent residence times on promoter DNA
552 indicating that photobleaching of molecules didn't significantly affect results.
553
554 **Single Molecule Co-localization Analysis**
555 Fluorescent spots in each frame for the movie of the promoter DNA, TFIID or p53 were mapped
556 using 2D Gaussian fitting methods (21, 57, 58) to determine the location (x, y) at subpixel
557 resolution. Co-localization analysis was performed as in (21) with the following modifications.
558 Coordinates of fluorescent spots were adjusted based upon movement of the fiducial marks (i.e.
559 reference beads) over time. Stage movement/drift was typically less than 200 nm over the time of
560 imaging (~20 minutes). Fluorescent spots that were located within 84 nm (1 pixel) throughout
561 the movie were grouped together in a cluster. The positions of all spots within a cluster were
562 averaged to obtain the overall location of an individual cluster of molecules. Position maps of the
563 clustered surface attached DNA molecules were then compared with position maps of either the

564 TFIID or p53 clusters. Clusters of TFIID or p53 molecules within 3 pixels (252 nm) of a DNA
565 cluster were found. Displacements of TFIID or p53 clustered molecules with a maximum equal
566 to (0,0) in the x and y positions are indicative of non-random co-localization between DNA and
567 TFIID or p53 clusters. Displacements between the x,y positions of the TFIID or p53 clusters and
568 the DNA clusters were then plotted as a 2D histogram with a bin size of 50 nm. 2D Gaussian
569 fitting of the 2D histogram yields σ which is equivalent to the variation in the displacement of
570 TFIID or p53 within 252 nm of a DNA molecule. A co-localization threshold was set to 1.8σ (84
571 nm).
572
573 **Single Molecule Residence Time Analysis of TFIID and p53 on promoter DNA**
574 For each TFIID or p53 cluster that co-localized with a DNA cluster (i.e. within 84 nm), we the
575 plotted the amplitude from the 2D Gaussian fit of every fluorescent spot within the TFIID or p53
576 cluster as a function of time. Homemade MATLAB software was then used to analyze the rise
577 and the fall of the amplitude of the fluorescent signal to determine the appearance and
578 corresponding disappearance of each spot over time. The residence time for each DNA binding
579 event is defined as the difference in time between the appearance and disappearance of a TFIID
580 or p53 fluorescent spot. The fluorescent signal from TFIID or p53 had to last for at least 1.5" to
581 be considered as a discrete binding event in our analysis. Due to rapid stochastic blinking of the
582 quantum dot, a dissociation event was only considered to have occurred if the quantum dot signal
583 remained in the off state longer than 4.5". At least 300 binding events of co-localized TFIID or
584 100 binding events of p53 clusters were analyzed for each particular promoter DNA construct.
585 For a subset of molecules (~100), the data was processed by hand to determine the appearance
586 and disappearance of fluorescent spots. Comparison of the residence times generated by our

587 automated software and by hand yielded negligible differences. Histograms of residence times
588 for TFIID or p53 bound to promoter DNA were fit to a two-component exponential decay model
589 to determine the average residence time of TFIID or p53 bound to promoter DNA (58). If the
590 difference between the fitted residence times for each individual component in the two-
591 component model varied less than 20%, histograms were re-fitted using a single-component
592 exponential decay model (58). For Figures 3 and S5 data was additionally fit to a gamma
593 distribution (38) via custom MATLAB software.
594
595 **2D Classification Analysis of TFIID co-complexes via negative stain EM**
596 4 μL (10-20 ng in total amount) of fresh TFIID/p53/bax DNA assemblies in 0.1M
597 KCl/HEMG buffer (20mM HEPES, 0.2 mM EDTA, 2mM $MgCl_2$, 10% Glucose [final pH 7.9])
598 was applied directly onto a thin carbon film supported by holey carbon on a 400-mesh copper
599 grid (Pacific Grid tech.) for 3', which was freshly glow-discharged. After incubating the sample
600 on the grid for 3', the sample grid was stained with five successive 75 μL drops of 1% Uranyl
601 Formate.
602 The negative stain image data were collected with a Tecnai F20 TWIN transmission
603 electron microscope operating at 120 keV at a calibrated magnification of 62,000x with a
604 defocus range of -0.5μm to -2.5μm using a Tietz F416 (4K x 4K) CCD camera (resulting in a
605 2.82 A/pixel) under the dosage 39.98 e^-/Å. A total of 14,000 particles (for TFIID alone), 13,855
606 particles (for TFIID/p53), and 19262 particles (for TFIID/p53/bax DNA) were manually picked
607 using Boxer (EMAN; (59)). These particles were aligned and classified in a reference-free
608 fashion as previously described (24) for 8 iterations. The similar measurement of Lobe's A
609 position relative to the lobes B and C was employed as in (26). Based upon the position of Lobe

610 A in relation to Lobe C v.s. Lobe B (26), three conformational groups of TFIID were defined
611 (i.e. canonical, transition, and rearranged state) in this study. The canonical form is represented
612 by Lobe A retaining its attachment to Lobe C. The transition state is represented by Lobe A
613 beginning to detach and move in between Lobe C and B. The rearranged form is represented by
614 Lobe A reattaching to Lobe B. Next, individual classums from the 5th , 6th, 7th and 8th iteration
615 for each TFIID/p53 prep with or without the *bax* DNA were examined carefully to select 2D
616 class averages displaying views of these three conformational groups. The number of 2D
617 averages in each conformational form v.s. total averages was calculated to yield the percentage
618 of TFIID's three conformations in each TFIID/p53 prep with or without the *bax* DNA. Three
619 independent protein purifications and EM data acquisition/analysis were performed to obtain the
620 standard deviation for the figure. A two sided student's T-test was used to determine statistical
621 significance.
622
623 **Cryo-EM data collection and image analysis**
624 For cryo-EM sample grid preparation, a thin carbon film supported by a 400-mesh carbon-
625 thickened C-flat holey grid with hole diameter 1.2 μm/spacing 1.3 μm (CF-1.2/1.3-4C,
626 Protochips) was plasma cleaned for 2 min using Denton high-vacuum evaporator. The grid was
627 loaded into a Vitrobot (FEI) that was preset at 100% humidity at 4ºC for vitrification of our
628 samples. 3 μl (504~900 ng in total amount) of the p53/TFIID/TFIIA/DNA assemblies was
629 applied directly onto the grid, incubated for 2 min and then blotted for 6.5 sec prior to plunge-
630 frozen in liquid ethane.
631 Cryo-EM data were collected with a JEM-2100F transmission electron microscope (JEOL)
632 operated at 120 KeV and at a magnification of 50,000x with a defocus range of –2.5 μm to –4.5

633 μm. Digital micrographs were collected using a TEM 2048x 2048 CCD camera (TemCam-
634 F224HD, TVIPS) with a pixel size of 24 μm and a calibrated magnification of 84,037x (2.86
635 Å/pixel) under low-dose conditions (~13 e^- /Å) via the semi-automatic image acquisition
636 SerialEM software (60). Digital micrographs showed homogeneous particles in terms of lack of
637 aggregation and apparent integrity of the intact complexes.

638 Particles were manually selected using boxer (EMAN) (59) for an initial total of 32,275
639 particles from the p53/TFIID/TFIIA/*bax* DNA dataset and 22,070 particles from the
640 p53/TFIID/TFIIA/*hdm2* DNA dataset. The particles were then phase flipped using CTF-
641 estimated values determined by CTFFIND3(61) and extracted using SPIDER (System for
642 Processing of Image Data from Electron microscopy and Related fields (62)) to a particle
643 window size of 128 x 128 pixels (5.72 Å/pixel), following the protocol as described in (26). The
644 particles were then normalized prior to the following data analyses. Reference-free 2D class
645 averaging image analysis was performed using IMAGIC (63) following the procedure precisely
646 as described (20). Using these 2D class averages as templates, we automatically picked particles
647 from a larger cryo-EM dataset using Signature (64) embedded in the Appion image processing
648 platform (65). A final total of 59,632 particles for the p53/TFIID/TFIIA/*bax* DNA co-complex
649 was obtained, normalized, and low-pass band filtered to perform the 3D reconstruction using
650 SPIDER's multi-reference projection matching approach as previously described (29). Both
651 rearranged and canonical forms of TFIID/TFIIA/SCP DNA from Eletron Microscopy Data Bank
652 (accession number 10832 and 10834, respectively) were filtered to 60 Å as a reference for the
653 first cycle of projection matching. Different initial reference models including TFIID alone, p53-
654 bound TFIID or TFIIA-bound TFIID were also tested for model bias refinement. New 3D
655 volumes reconstructed from the data set were used as references for all subsequent cycles of

656 alignment (angular step sizes ranging from an initial 20° to a final 2°). The resolution throughout
657 the refinement was determined by the 0.5 cut-off in the Fourier shell correlation (FSC) curve.
658 The 3D structure of the p53/TFIID/TFIIA/bax assembly was filtered at a final resolution ~35 Å.
659 All the 3D reconstructions were represented as isodensity surfaces using the UCSF Chimera
660 package (66) developed by the Resource for Biocomputing, Visualization, and Informatics at the
661 University of California, San Francisco (supported by NIH NIGMS P41-GM103311).
662
663
664
665
666

Funding information

This study was supported by start up funds (Albert Einstein College of Medicine) and NIH/NIBIB 1U01EB021236-02. Some of this work was performed at the Simons Electron Microscopy Center at the New York Structural Biology Center that is supported by a grant from the Simons Foundation (Grant Number: 349247) with additional support from: NIH S10 OD019994-01, the Agouron Institute (Grant Number: F00316), NIH S10 RR029300-01, NIH S10 RR017291-01, NYSTAR, and NIH C06 RR017528-01-CEM.

Acknowledgement

We specifically thank R. Tjian, S. Chu, and E. Nogales for their initial support of this study, S. Zheng for generating TAF4 mAb supernatant and HeLa cells, D. King for providing the TAF4 mAb elution peptide, A. Revyakin, A. Pertsinidis and S.R. Park for their help on initial stages of the single molecule microscopy, and R. Henderson for his technical advice critical for the cryo-EM work. We also thank S.M. Shenoy, J. Hargitai, J. Wang, S. Lenny, J. Greally and E. Eng for high performance computing cluster and cryo-EM technical support. We appreciate assistance from Einstein's AIF facility, especially F. P. Macaluso, L. Cummins and G. S. Perumal. We are grateful to M. Keogh, Charles Kenworthy and E. Nogales for critical comments of the manuscript. W. Liu is an affiliated member of the New York Structural Biology Center. M. Cianfrocco is an HHMI fellow of the Damon Runyon Cancer Research Foundation.

688 **Figure legends**

689 **Figure 1. Single Molecule Total Internal Reflection Fluorescence (TIRF) Microscopy**
690 **analysis of Quantum dot-labeled TFIID binding of promoter DNA in vitro.** (A) Schematic
691 representation of an in vitro single molecule TIRF assay to monitor binding of quantum dot
692 (QD)-labeled TFIID to fluorescently labeled *bax* or *hdm2* promoter DNA in real-time. (B)
693 Dependence of TFIID/promoter DNA co-localization on p53, the p53 RE, and core promoter
694 elements. Promoter DNA binding is plotted as a percentage of total DNA molecules in a field of
695 view that are co-localized with TFIID over 15' of binding based on TFIID–promoter DNA
696 displacement histograms. A co-localization threshold of 84 nm was set based upon our previous
697 study (21). TFIID binding to wild-type *bax* DNA is compared with and without p53. Additional
698 comparisons were made for TFIID binding to wild-type (WT), Mutant p53 RE (Mu RE), Mutant
699 Core (Mu Core), or combined mutant RE and core (Mu RE/Co) *hdm2* DNA templates. (C) xlink-
700 Exo analysis of TFIID binding to wild-type (top panel) and Mu RE/Co (bottom panel) *hdm2*
701 DNA. Basepair annotations (+/- 2bp) above individual peaks in the line traces (right panel)
702 represent a -4bp adjustment to reflect the known inability of Exonuclease to cut immediately
703 adjacent to protein/DNA crosslink sites (32).

704

705 **Figure 2. Residence time analysis of TFIID bound to promoter DNA.** (A) Traces of
706 individual co-localized TFIID/promoter DNA binding events were further analyzed to determine
707 TFIID's average residence time. TFIID displays a mixture of short (left panel) and long-lived
708 (right panel) binding events. (B) 1–Cumulative Distribution Function Plots (1–CDF) of TFIID
709 bound to DNA in the absence (left panel) and presence (right panel) of p53 were fitted to a single
710 (gray dashed) or two-component (red solid) exponential decay model. Fitting analysis reveals
711 that TFIID complexes bound to promoter DNA display residence times comprised of a long- ($\tau 1$)

712 and a short- (τ2) lived component. Percentages of the long- (τ1) and short- (τ2) lived
713 components are listed next to the residence time. (C) Bar graph comparing TFIID's average
714 short- and long-binding in the absence and presence of p53. (D) Percentage of short and long-
715 lived TFIID binding events on the wild-type (RE), mutant RE (Mu RE), mutant Core (Mu Core)
716 and mutant RE/Core (Mu RE/Co) *hdm2* promoter DNA. * = p-value < 0.05, *** = p-value <
717 0.001, N.S. = Not significant.
718
719 **Figure 3. Residence time analysis of p53 bound to promoter DNA with and without TFIID.**
720 (A) Individual co-localized p53/promoter DNA binding events were further analyzed to
721 determine the average residence time for p53 bound to wild-type (left panel) and Mutant p53 RE
722 (right panel) *hdm2* promoter DNA. 1−Cumulative Distribution Function Plots (1−CDF) of p53
723 bound to promoter DNA were fit to a single (gray dashed) or two (red solid)-component
724 exponential decay model. Based on comparisons of the *hdm2* promoter DNAs containing wild-
725 type and mutant p53 REs, τ1 represents specific binding of p53 to the wild-type *hdm2* DNA
726 while τns equals non-specific interactions between p53 and promoter DNA. (B) 1−CDF plots of
727 p53 bound to the wild-type *hdm2* DNA template in the presence of TFIID were fit to a single
728 (gray dashed) and two (red solid)-component exponential decay (left panel) or gamma
729 distribution (right panel) model. (C) Bar graph of p53's residence time in the absence and
730 presence of TFIID bound to the wild-type *hdm2* DNA (left panel). Residence time analysis of
731 TFIID and p53 bound to the wild-type *hdm2* DNA (right panel).
732
733 **Figure 4. Structural EM analysis on p53's impact on TFIID bound to native target gene**
734 **promoters.** (A) TFIID's structural plasticity as defined by the position of its Lobe A (26)(top

735 panels, the major lobes of TFIID are labeled as A, B, and C). TFIID's conformations are
736 classified into three groups: Canonical, Transition and Rearranged state as shown. Reference-
737 free 2D classification analysis on negative stain EM datasets showing populations of different
738 TFIID conformations in the absence of p53 (gray), presence of p53 (white), and with p53 + *bax*
739 DNA (black). The scale bar represents 100Å. (B) Three representative reference-free 2D class
740 averages of p53/TFIID/TFIIA bound to either the *bax* or *hdm2* DNA are shown based upon cryo-
741 EM particle datasets. The scale bar is 200Å. (C) Distinct 2D class averages showing views of the
742 assemblies bound to the *bax* promoter DNA fragment downstream (top panel, DNA highlighted
743 in green arrows) and upstream (middle panel, DNA highlighted in yellow arrows) of the
744 transcription start site (TSS, +1) are presented respectively. The orientation of the core promoter
745 elements bound by TFIID were previously mapped in the 3D structure of TFIID/TFIIA bound to
746 the super-core promoter (SCP) DNA (26). The corresponding views of the 3D structure of
747 TFIID/TFIIA/SCP DNA are shown (far right) to indicate the DNA orientation. The strong 3D
748 density highlighted in green represents the promoter DNA comprising the initiator, TSS and
749 downstream promoter elements. Since the upstream promoter DNA was weakly visible, focused
750 classification analysis (bottom panel) were performed using those corresponding class averages
751 (middle panel) to clarify the presence of the *bax* promoter DNA upstream of the TATA box
752 (highlighted by yellow arrow). The scale bar is 200Å.
753
754 **Figure 5. A representative model of how TFIID engages the core promoter at various p53-**
755 **responsive promoters.** A proposed model of how p53 aids TFIID in core promoter recognition
756 is presented based upon our current and previous studies (20). In the absence of p53, TFIID
757 primarily exists in the canonical conformation which is weakly permissive for DNA binding due

758 in part to interactions between the TAF1 TAND and TBP. The canonical form of TFIID can
759 infrequently and transiently interact with DNA. In rare occurances, canonical TFIID isomerizes
760 to a structurally rearranged form that involves severance of TAF1 TAND/TBP contacts and
761 movement of TBP from lobe A/C to lobe B. In the presence of p53, the TBP/TAF1 TAND
762 interaction is disrupted leading to a TFIID complex that is highly permissive to isomerization
763 and stable DNA binding. Once TFIID structurally rearranges and binds DNA via movement of
764 TBP from lobe A/C to lobe B, p53 disengages TFIID through loss of its contacts with Lobe A
765 and C. Dissociation of p53 from the TFIID/promoter DNA scaffold results in "recycling" of the
766 p53 RE for further assembly of the PIC components.
767
768
769

769 **References**

770

771 1. **Menendez D, Inga A, Resnick MA.** 2009. The expanding universe of p53 targets.
772 Nat Rev Cancer **9:**724-737.
773 2. **Bieging KT, Mello SS, Attardi LD.** 2014. Unravelling mechanisms of p53-mediated
774 tumour suppression. Nat Rev Cancer **14:**359-370.
775 3. **Tafvizi A, Huang F, Fersht AR, Mirny LA, van Oijen AM.** 2011. A single-molecule
776 characterization of p53 search on DNA. Proc Natl Acad Sci U S A **108:**563-568.
777 4. **Lu H, Levine AJ.** 1995. Human TAFII31 protein is a transcriptional coactivator of
778 the p53 protein. Proc Natl Acad Sci U S A **92:**5154-5158.
779 5. **Thut CJ, Chen JL, Klemm R, Tjian R.** 1995. p53 transcriptional activation mediated
780 by coactivators TAFII40 and TAFII60. Science **267:**100-104.
781 6. **Buschmann T, Lin Y, Aithmitti N, Fuchs SY, Lu H, Resnick-Silverman L,**
782 **Manfredi JJ, Ronai Z, Wu X.** 2001. Stabilization and activation of p53 by the
783 coactivator protein TAFII31. J Biol Chem **276:**13852-13857.
784 7. **Li AG, Piluso LG, Cai X, Gadd BJ, Ladurner AG, Liu X.** 2007. An acetylation switch
785 in p53 mediates holo-TFIID recruitment. Mol Cell **28:**408-421.
786 8. **Juven-Gershon T, Hsu JY, Kadonaga JT.** 2006. Perspectives on the RNA
787 polymerase II core promoter. Biochem Soc Trans **34:**1047-1050.
788 9. **Colgan J, Manley JL.** 1992. TFIID can be rate limiting in vivo for TATA-containing,
789 but not TATA-lacking, RNA polymerase II promoters. Genes Dev **6:**304-315.
790 10. **Chi T, Carey M.** 1996. Assembly of the isomerized TFIIA--TFIID--TATA ternary
791 complex is necessary and sufficient for gene activation. Genes Dev **10:**2540-2550.
792 11. **Wang W, Gralla JD, Carey M.** 1992. The acidic activator GAL4-AH can stimulate
793 polymerase II transcription by promoting assembly of a closed complex requiring
794 TFIID and TFIIA. Genes Dev **6:**1716-1727.
795 12. **White J, Brou C, Wu J, Lutz Y, Moncollin V, Chambon P.** 1992. The acidic
796 transcriptional activator GAL-VP16 acts on preformed template-committed
797 complexes. Embo J **11:**2229-2240.
798 13. **Chi T, Carey M.** 1993. The ZEBRA activation domain: modular organization and
799 mechanism of action. Mol Cell Biol **13:**7045-7055.
800 14. **Lieberman PM, Berk AJ.** 1994. A mechanism for TAFs in transcriptional activation:
801 activation domain enhancement of TFIID-TFIIA--promoter DNA complex formation.
802 Genes Dev **8:**995-1006.
803 15. **Chi T, Lieberman P, Ellwood K, Carey M.** 1995. A general mechanism for
804 transcriptional synergy by eukaryotic activators. Nature **377:**254-257.
805 16. **Kobayashi N, Boyer TG, Berk AJ.** 1995. A class of activation domains interacts
806 directly with TFIIA and stimulates TFIIA-TFIID-promoter complex assembly. Mol
807 Cell Biol **15:**6465-6473.
808 17. **Rhee HS, Pugh BF.** 2012. Genome-wide structure and organization of eukaryotic
809 pre-initiation complexes. Nature **483:**295-301.
810 18. **Lieberman PM, Ozer J, Gursel DB.** 1997. Requirement for transcription factor IIA
811 (TFIIA)-TFIID recruitment by an activator depends on promoter structure and
812 template competition. Mol Cell Biol **17:**6624-6632.

813 19. **Xing J, Sheppard HM, Corneillie SI, Liu X.** 2001. p53 Stimulates TFIID-TFIIA-
814 promoter complex assembly, and p53-T antigen complex inhibits TATA binding
815 protein-TATA interaction. Mol Cell Biol **21:**3652-3661.
816 20. **Liu WL, Coleman RA, Ma E, Grob P, Yang JL, Zhang Y, Dailey G, Nogales E, Tjian**
817 **R.** 2009. Structures of three distinct activator-TFIID complexes. Genes Dev **23:**1510-
818 1521.
819 21. **Revyakin A, Zhang Z, Coleman RA, Li Y, Inouye C, Lucas JK, Park SR, Chu S, Tjian**
820 **R.** 2012. Transcription initiation by human RNA polymerase II visualized at single-
821 molecule resolution. Genes Dev **26:**1691-1702.
822 22. **Zhang Z, English BP, Grimm JB, Kazane SA, Hu W, Tsai A, Inouye C, You C,**
823 **Piehler J, Schultz PG, Lavis LD, Revyakin A, Tjian R.** 2016. Rapid dynamics of
824 general transcription factor TFIIB binding during preinitiation complex assembly
825 revealed by single-molecule analysis. Genes Dev **30:**2106-2118.
826 23. **Tantale K, Mueller F, Kozulic-Pirher A, Lesne A, Victor JM, Robert MC, Capozi S,**
827 **Chouaib R, Backer V, Mateos-Langerak J, Darzacq X, Zimmer C, Basyuk E,**
828 **Bertrand E.** 2016. A single-molecule view of transcription reveals convoys of RNA
829 polymerases and multi-scale bursting. Nat Commun **7:**12248.
830 24. **Liu WL, Coleman RA, Grob P, King DS, Florens L, Washburn MP, Geles KG, Yang**
831 **JL, Ramey V, Nogales E, Tjian R.** 2008. Structural changes in TAF4b-TFIID correlate
832 with promoter selectivity. Mol Cell **29:**81-91.
833 25. **Papai G, Tripathi MK, Ruhlmann C, Layer JH, Weil PA, Schultz P.** 2010. TFIIA and
834 the transactivator Rap1 cooperate to commit TFIID for transcription initiation.
835 Nature **465:**956-960.
836 26. **Cianfrocco MA, Kassavetis GA, Grob P, Fang J, Juven-Gershon T, Kadonaga JT,**
837 **Nogales E.** 2013. Human TFIID binds to core promoter DNA in a reorganized
838 structural state. Cell **152:**120-131.
839 27. **Louder RK, He Y, Lopez-Blanco JR, Fang J, Chacon P, Nogales E.** 2016. Structure
840 of promoter-bound TFIID and model of human pre-initiation complex assembly.
841 Nature **531:**604-609.
842 28. **Andel F, 3rd, Ladurner AG, Inouye C, Tjian R, Nogales E.** 1999. Three-
843 dimensional structure of the human TFIID-IIA-IIB complex. Science **286:**2153-2156.
844 29. **Grob P, Cruse MJ, Inouye C, Peris M, Penczek PA, Tjian R, Nogales E.** 2006. Cryo-
845 electron microscopy studies of human TFIID: conformational breathing in the
846 integration of gene regulatory cues. Structure **14:**511-520.
847 30. **Bourdon JC, Deguin-Chambon V, Lelong JC, Dessen P, May P, Debuire B, May E.**
848 1997. Further characterisation of the p53 responsive element--identification of new
849 candidate genes for trans-activation by p53. Oncogene **14:**85-94.
850 31. **Juven-Gershon T, Cheng S, Kadonaga JT.** 2006. Rational design of a super core
851 promoter that enhances gene expression. Nat Methods **3:**917-922.
852 32. **Chang GS, Chen XA, Park B, Rhee HS, Li P, Han KH, Mishra T, Chan-Salis KY, Li Y,**
853 **Hardison RC, Wang Y, Pugh BF.** 2014. A Comprehensive and High-Resolution
854 Genome-wide Response of p53 to Stress. Cell Rep **8:**514-527.
855 33. **Galasinski SK, Lively TN, Grebe De Barron A, Goodrich JA.** 2000. Acetyl
856 coenzyme A stimulates RNA polymerase II transcription and promoter binding by
857 transcription factor IID in the absence of histones. Mol Cell Biol **20:**1923-1930.

858 34. **Zhang Z, Boskovic Z, Hussain MM, Hu W, Inouye C, Kim HJ, Abole AK, Doud MK,**
859 **Lewis TA, Koehler AN, Schreiber SL, Tjian R.** 2015. Chemical perturbation of an
860 intrinsically disordered region of TFIID distinguishes two modes of transcription
861 initiation. Elife **4**.
862 35. **Mazur SJ, Sakaguchi K, Appella E, Wang XW, Harris CC, Bohr VA.** 1999.
863 Preferential binding of tumor suppressor p53 to positively or negatively supercoiled
864 DNA involves the C-terminal domain. J Mol Biol **292:**241-249.
865 36. **Weinberg RL, Freund SM, Veprintsev DB, Bycroft M, Fersht AR.** 2004. Regulation
866 of DNA binding of p53 by its C-terminal domain. J Mol Biol **342:**801-811.
867 37. **Emamzadah S, Tropia L, Vincenti I, Falquet B, Halazonetis TD.** 2014. Reversal of
868 the DNA-binding-induced loop L1 conformational switch in an engineered human
869 p53 protein. J Mol Biol **426:**936-944.
870 38. **Floyd DL, Harrison SC, van Oijen AM.** 2010. Analysis of kinetic intermediates in
871 single-particle dwell-time distributions. Biophys J **99:**360-366.
872 39. **Miyashita T, Reed JC.** 1995. Tumor suppressor p53 is a direct transcriptional
873 activator of the human bax gene. Cell **80:**293-299.
874 40. **Phelps M, Darley M, Primrose JN, Blaydes JP.** 2003. p53-independent activation
875 of the hdm2-P2 promoter through multiple transcription factor response elements
876 results in elevated hdm2 expression in estrogen receptor alpha-positive breast
877 cancer cells. Cancer Res **63:**2616-2623.
878 41. **Liu D, Ishima R, Tong KI, Bagby S, Kokubo T, Muhandiram DR, Kay LE,**
879 **Nakatani Y, Ikura M.** 1998. Solution structure of a TBP-TAF(II)230 complex:
880 protein mimicry of the minor groove surface of the TATA box unwound by TBP. Cell
881 **94:**573-583.
882 42. **Anandapadamanaban M, Andresen C, Helander S, Ohyama Y, Siponen MI,**
883 **Lundstrom P, Kokubo T, Ikura M, Moche M, Sunnerhagen M.** 2013. High-
884 resolution structure of TBP with TAF1 reveals anchoring patterns in transcriptional
885 regulation. Nat Struct Mol Biol **20:**1008-1014.
886 43. **Kokubo T, Gong DW, Yamashita S, Horikoshi M, Roeder RG, Nakatani Y.** 1993.
887 Drosophila 230-kD TFIID subunit, a functional homolog of the human cell cycle gene
888 product, negatively regulates DNA binding of the TATA box-binding subunit of
889 TFIID. Genes Dev **7:**1033-1046.
890 44. **Kokubo T, Yamashita S, Horikoshi M, Roeder RG, Nakatani Y.** 1994. Interaction
891 between the N-terminal domain of the 230-kDa subunit and the TATA box-binding
892 subunit of TFIID negatively regulates TATA-box binding. Proc Natl Acad Sci U S A
893 **91:**3520-3524.
894 45. **Lively TN, Ferguson HA, Galasinski SK, Seto AG, Goodrich JA.** 2001. c-Jun binds
895 the N terminus of human TAF(II)250 to derepress RNA polymerase II transcription
896 in vitro. J Biol Chem **276:**25582-25588.
897 46. **Lively TN, Nguyen TN, Galasinski SK, Goodrich JA.** 2004. The basic leucine zipper
898 domain of c-Jun functions in transcriptional activation through interaction with the
899 N terminus of human TATA-binding protein-associated factor-1 (human
900 TAF(II)250). J Biol Chem **279:**26257-26265.
901 47. **Kokubo T, Swanson MJ, Nishikawa JI, Hinnebusch AG, Nakatani Y.** 1998. The
902 yeast TAF145 inhibitory domain and TFIIA competitively bind to TATA-binding
903 protein. Mol Cell Biol **18:**1003-1012.

904 48. **Ozer J, Mitsouras K, Zerby D, Carey M, Lieberman PM.** 1998. Transcription factor
905 IIA derepresses TATA-binding protein (TBP)-associated factor inhibition of TBP-
906 DNA binding. J Biol Chem **273:**14293-14300.
907 49. **Xiao H, Pearson A, Coulombe B, Truant R, Zhang S, Regier JL, Triezenberg SJ,**
908 **Reinberg D, Flores O, Ingles CJ, et al.** 1994. Binding of basal transcription factor
909 TFIIH to the acidic activation domains of VP16 and p53. Mol Cell Biol **14:**7013-7024.
910 50. **Gazit K, Moshonov S, Elfakess R, Sharon M, Mengus G, Davidson I, Dikstein R.**
911 2009. TAF4/4b x TAF12 displays a unique mode of DNA binding and is required for
912 core promoter function of a subset of genes. J Biol Chem **284:**26286-26296.
913 51. **Liu X, Berk AJ.** 1995. Reversal of in vitro p53 squelching by both TFIIB and TFIID.
914 Mol Cell Biol **15:**6474-6478.
915 52. **Espinosa JM, Verdun RE, Emerson BM.** 2003. p53 functions through stress- and
916 promoter-specific recruitment of transcription initiation components before and
917 after DNA damage. Mol Cell **12:**1015-1027.
918 53. **Singh SK, Qiao Z, Song L, Jani V, Rice W, Eng E, Coleman RA, Liu WL.** 2016.
919 Structural visualization of the p53/RNA polymerase II assembly. Genes Dev
920 **30:**2527-2537.
921 54. **Okuda M, Nishimura Y.** 2015. Real-time and simultaneous monitoring of the
922 phosphorylation and enhanced interaction of p53 and XPC acidic domains with the
923 TFIIH p62 subunit. Oncogenesis **4:**e150.
924 55. **Leveillard T, Andera L, Bissonnette N, Schaeffer L, Bracco L, Egly JM, Wasylyk**
925 **B.** 1996. Functional interactions between p53 and the TFIIH complex are affected by
926 tumour-associated mutations. EMBO J **15:**1615-1624.
927 56. **Poorey K, Viswanathan R, Carver MN, Karpova TS, Cirimotich SM, McNally JG,**
928 **Bekiranov S, Auble DT.** 2013. Measuring chromatin interaction dynamics on the
929 second time scale at single-copy genes. Science **342:**369-372.
930 57. **Huang B, Jones SA, Brandenburg B, Zhuang X.** 2008. Whole-cell 3D STORM
931 reveals interactions between cellular structures with nanometer-scale resolution.
932 Nat Methods **5:**1047-1052.
933 58. **Chen J, Zhang Z, Li L, Chen BC, Revyakin A, Hajj B, Legant W, Dahan M, Lionnet**
934 **T, Betzig E, Tjian R, Liu Z.** 2014. Single-molecule dynamics of enhanceosome
935 assembly in embryonic stem cells. Cell **156:**1274-1285.
936 59. **Ludtke SJ, Baldwin PR, Chiu W.** 1999. EMAN: semiautomated software for high-
937 resolution single-particle reconstructions. J Struct Biol **128:**82-97.
938 60. **Mastronarde DN.** 2005. Automated electron microscope tomography using robust
939 prediction of specimen movements. J Struct Biol **152:**36-51.
940 61. **Mindell JA, Grigorieff N.** 2003. Accurate determination of local defocus and
941 specimen tilt in electron microscopy. J Struct Biol **142:**334-347.
942 62. **Shaikh TR, Gao H, Baxter WT, Asturias FJ, Boisset N, Leith A, Frank J.** 2008.
943 SPIDER image processing for single-particle reconstruction of biological
944 macromolecules from electron micrographs. Nat Protoc **3:**1941-1974.
945 63. **van Heel M, Harauz G, Orlova EV, Schmidt R, Schatz M.** 1996. A new generation of
946 the IMAGIC image processing system. J Struct Biol **116:**17-24.
947 64. **Chen JZ, Grigorieff N.** 2007. SIGNATURE: a single-particle selection system for
948 molecular electron microscopy. J Struct Biol **157:**168-173.

949 65. **Lander GC, Stagg SM, Voss NR, Cheng A, Fellmann D, Pulokas J, Yoshioka C,**
950 **Irving C, Mulder A, Lau PW, Lyumkis D, Potter CS, Carragher B.** 2009. Appion: an
951 integrated, database-driven pipeline to facilitate EM image processing. J Struct Biol
952 **166:**95-102.
953 66. **Pettersen EF, Goddard TD, Huang CC, Couch GS, Greenblatt DM, Meng EC,**
954 **Ferrin TE.** 2004. UCSF Chimera--a visualization system for exploratory research
955 and analysis. J Comput Chem **25:**1605-1612.
956

Coleman_Fig. 1

Figure 1

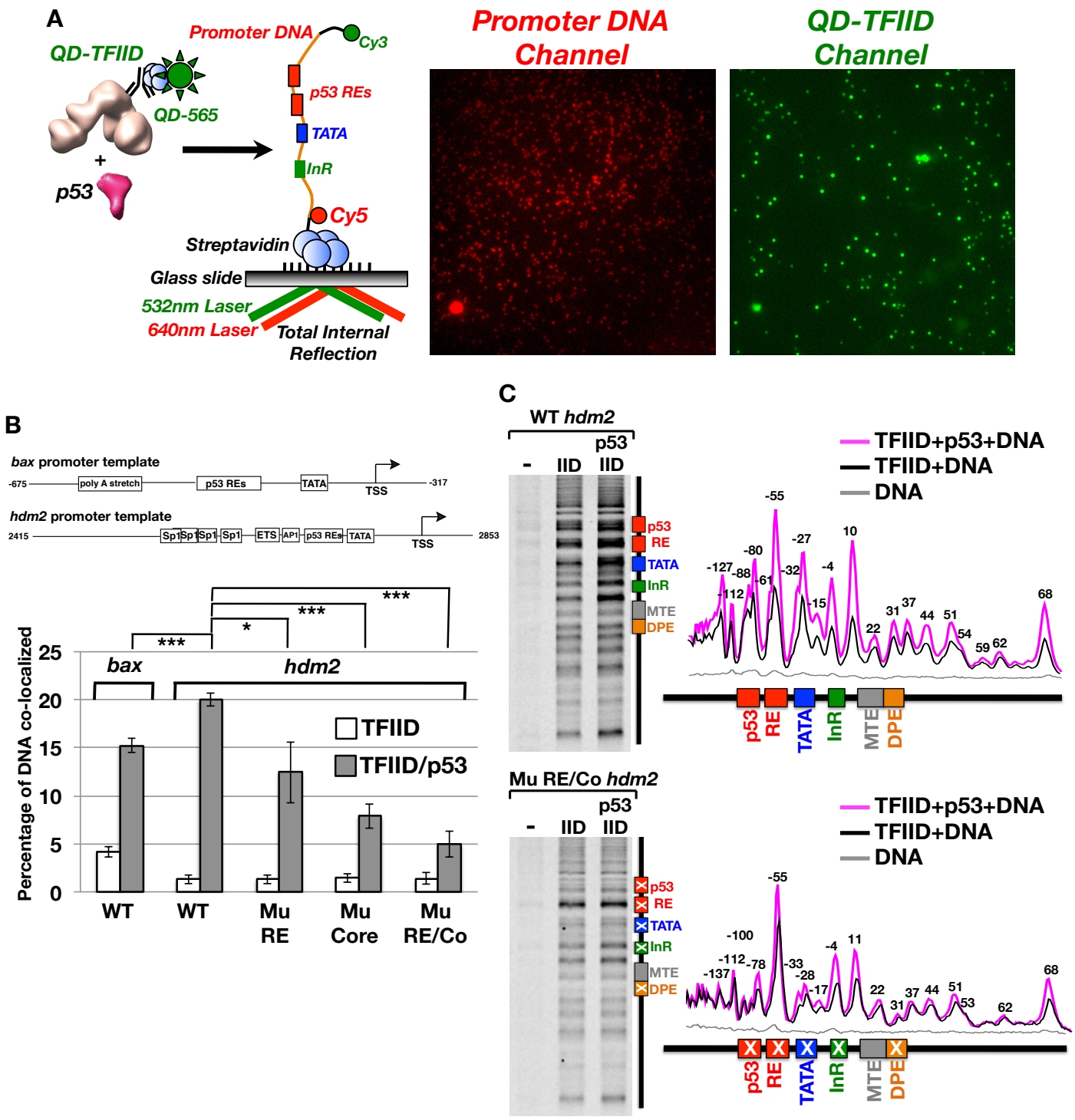

Coleman_Fig. 2

Figure 2

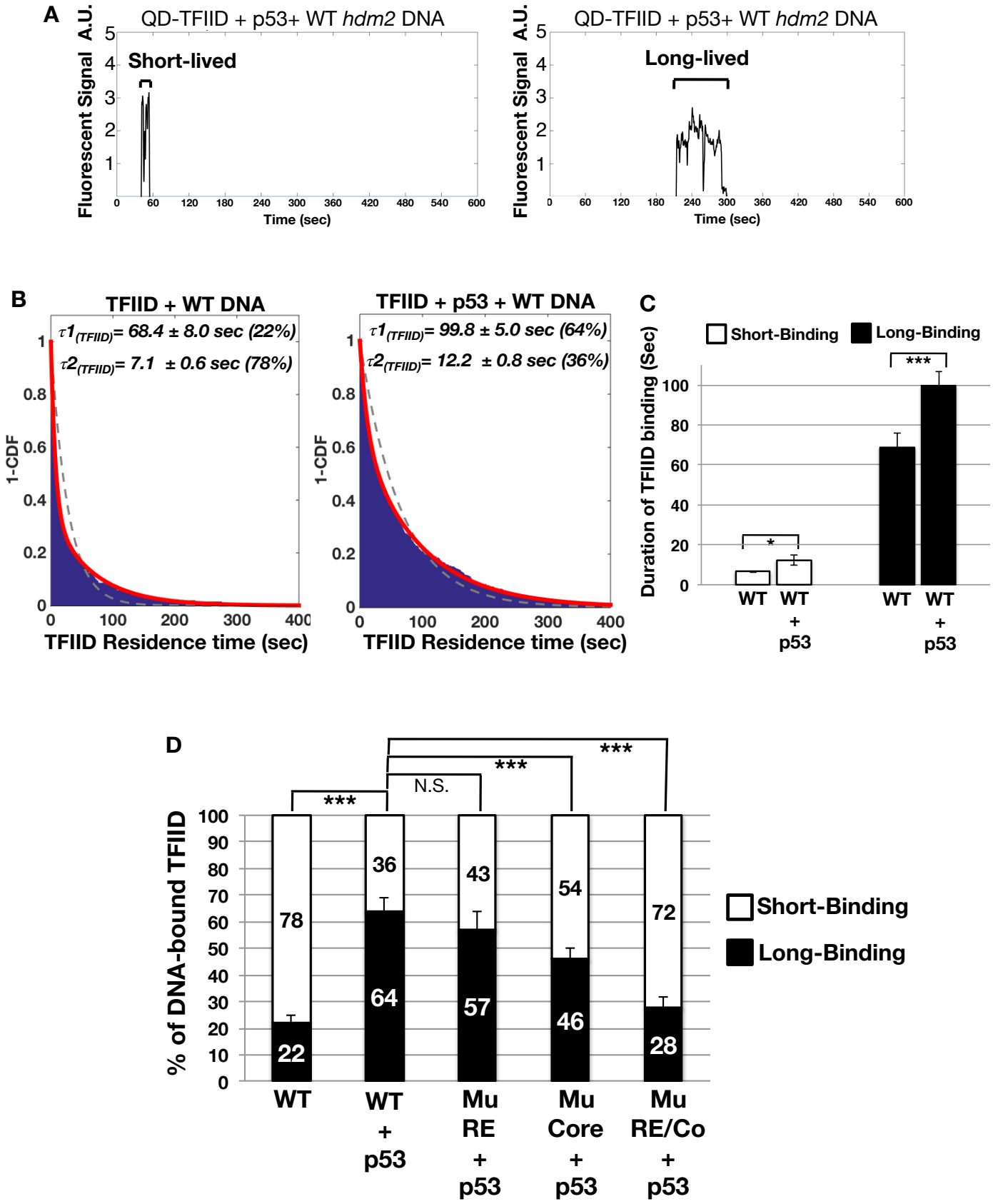

Figure 3

Coleman_Fig. 3

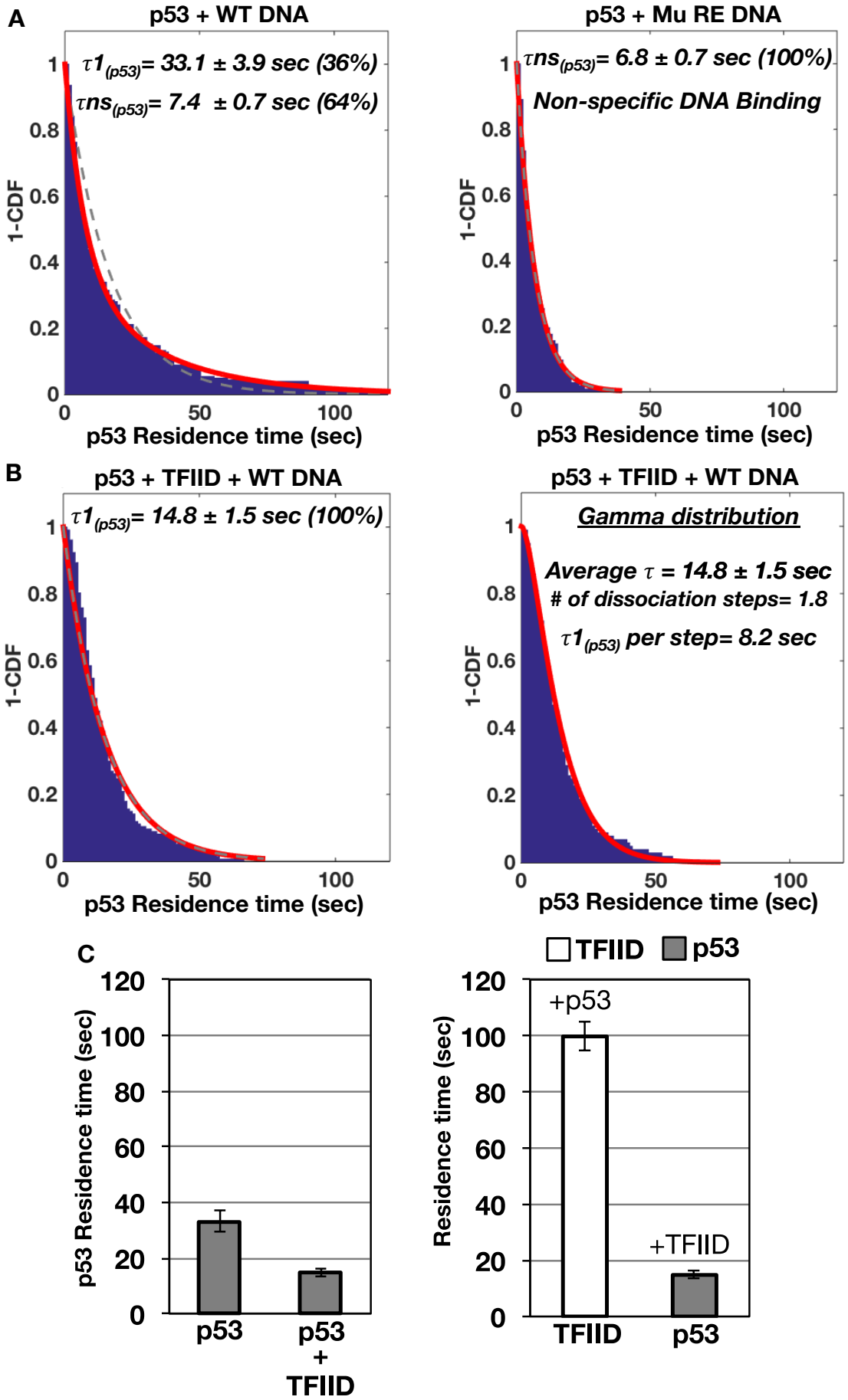

Figure 4

Coleman_Fig. 4

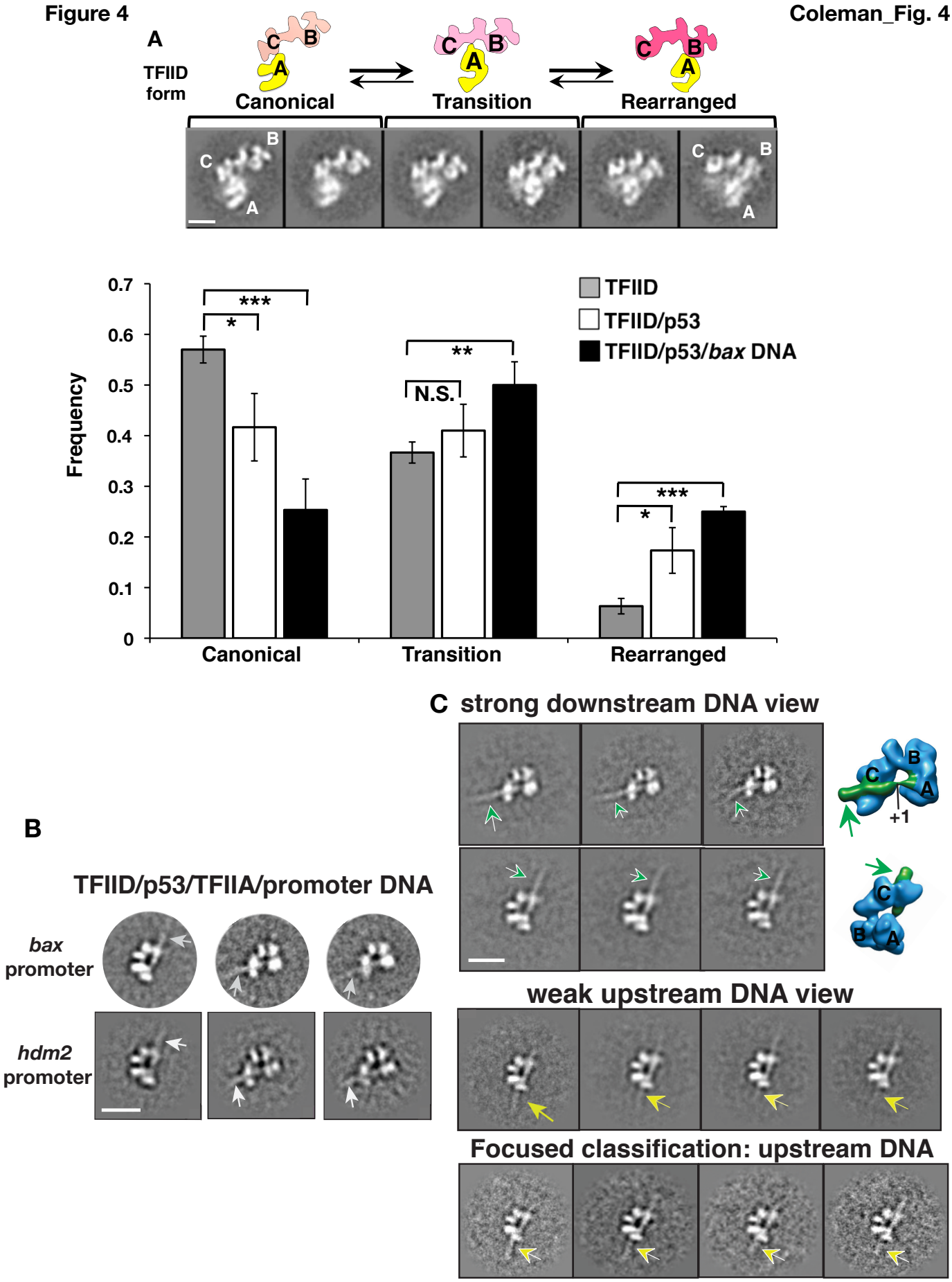

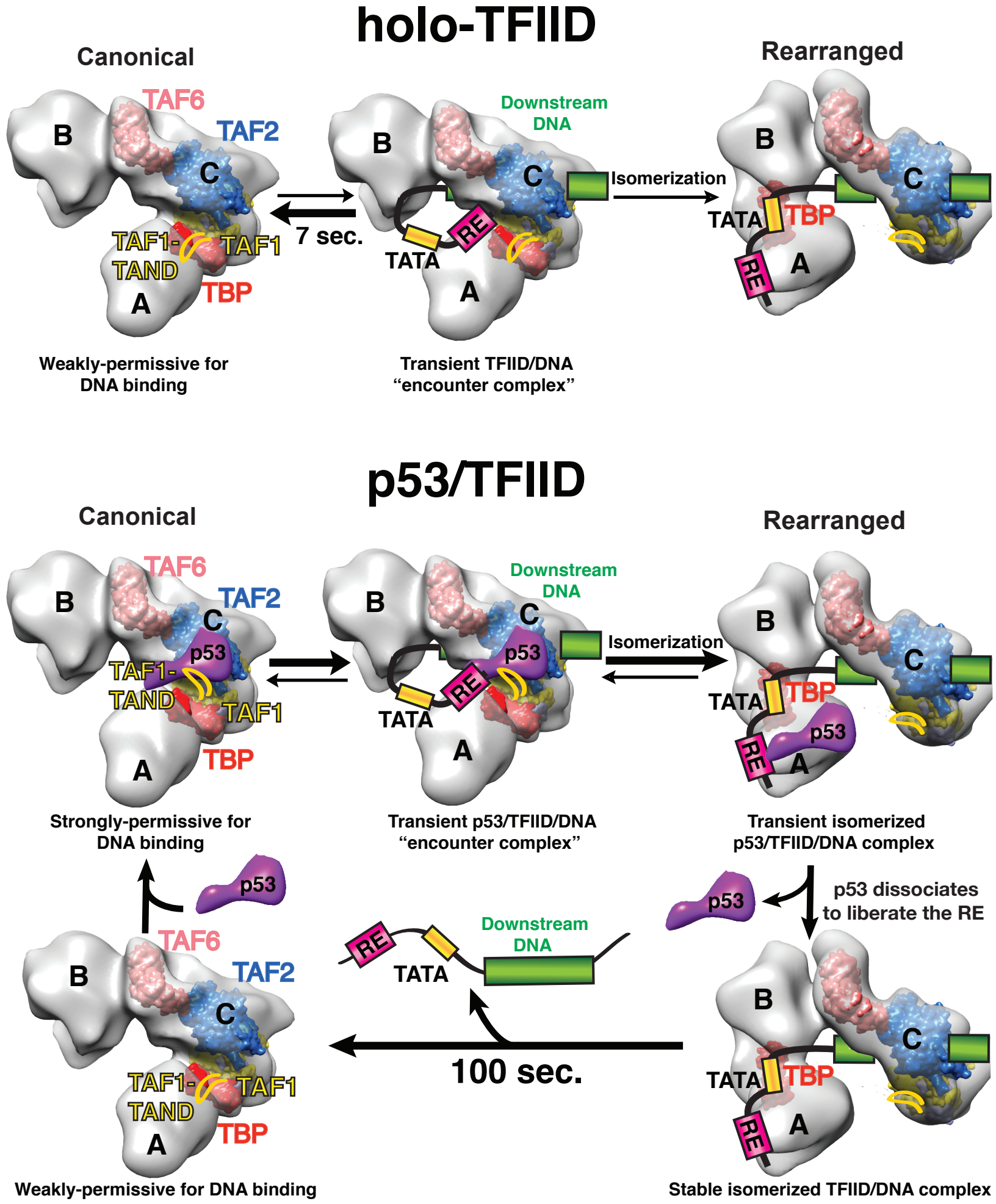
holo-TFIID
Canonical
Rearranged
TAF6
TAF2
B
C
TAF1-
TAND
TAF1
TBP
A
7 sec.
Downstream
DNA
RE
TATA
Isomerization
TATA
TBP
Weakly-permissive for
DNA binding
Transient TFIID/DNA
"encounter complex"
p53/TFIID
Canonical
Rearranged
p53
Strongly-permissive for
DNA binding
Transient p53/TFIID/DNA
"encounter complex"
Transient isomerized
p53/TFIID/DNA complex
p53 dissociates
to liberate the RE
100 sec.
Weakly-permissive for DNA binding
Stable isomerized TFIID/DNA complex